Implementation and Validation of a Data-Driven Variable Impedance Controller on the Össur Power Knee

T. Kevin Best[1], C. Andrew Seelhoff[2], and Robert D. Gregg[1,2]

***Abstract*—While prototype prostheses and control algorithms have demonstrated compelling clinical benefits in research laboratories, studies with commercially-available robotic prostheses have often failed to demonstrate similar benefits for users, limiting their adoption into mainstream clinical practice. This work is a step towards addressing this shortcoming by presenting the implementation of a phase-based variable impedance controller on the commercially-available Össur Power Knee™ for walking and sit/stand tasks. We show that, through preliminary experiments with N=4 high-mobility above-knee prosthesis users, the Power Knee under our controller can produce clear clinical benefits compared to the users' prescribed prostheses. In sitting and standing, users demonstrated generally increased leg-loading symmetry and speed with the Power Knee, indicating easier motions with less over-use of the sound limb. In walking, users demonstrated improved gait with the Power Knee, including increases in toe clearance and early-stance knee flexion. These positive results are similar to our previous work on prototype hardware, demonstrating our controller's hardware generalization and its potential for generating clinical benefits with commercial prostheses. These results are a step towards a promising future in which commercially-available robotic prostheses provide users with concrete clinical benefits.**

I. Introduction

Robotic knee prostheses have been slow to gain widespread adoption in clinical practice, despite their many promised benefits [1], [2]. In research laboratories, prototype robotic knee-ankle prostheses have been shown to enable more normative joint biomechanics [3]–[5], improve inter-limb symmetry [3], [6]–[8], reduce energy expenditure [9], [10], and, in some cases, improve user endurance [11]. However, translating these technologies into clear clinical benefits with commercialized robotic knee prostheses, such as the Össur Power Knee™ (Reykjavík, Iceland), has historically been a challenge [12]–[14].

In addition to energy, weight, noise, and cost concerns, the limited adoption of robotic knees in clinical practice is likely due to challenges in designing their control systems. A commercial prosthesis must be extremely robust, predictable, and easy to use, often leading manufacturers to elect to use simple and conservative discrete control approaches, such as the seminal finite state machine (FSM) impedance controller [15]. An FSM impedance controller uses distinct impedance parameters in a sequence of discrete gait phases, which are uniquely defined for each discrete activity mode. While these types of controllers can be quite effective in their intended conditions, optimal performance often requires extensive tuning by trained experts [16]. This poses a problem for clinical deployment, as clinicians often lack both the time and technical expertise to optimally configure these controllers, potentially resulting in sub-optimal configurations and subsequent user outcomes. It is likely that, even with the same hardware, better user outcomes could be more consistently achievable either through automated parameter tuning [17], [18], or by using alternative control strategies with lesser tuning requirements. Additionally, better outcomes may be achievable with controllers that can automatically adapt to continuous variations in the user's activity (*e.g.,* walking speed or ground incline).

Our research group has worked towards addressing these challenges through the development of a continuous, data-driven control framework known as hybrid kinematic impedance control (HKIC). These controllers encode information from large biomechanics datasets of able-bodied (AB) individuals performing various activities of daily living (ADLs) [19]–[21], utilizing continuous gait phase and task estimates to synchronize with the user and to adapt prosthesis behavior to suit the current terrain. We have applied this control framework for walking at variable speeds and inclines [5], [22], stair ascent and descent at different step heights [23], [24], and transitioning to/from sitting with different chair heights [8]. When deployed on our high-torque, low-inertia prototype powered knee-ankle prosthesis [25], these controllers have been shown to produce clinical benefits such as biomimetic joint mechanics [5], [8], [23], improved symmetry [8], reduced toe stubbing [26], and improved endurance [11].

This data-driven control approach is attractive for use in clinical settings, as it would, in theory, allow users to realize these clinical benefits across a continuum of ambulation tasks without imposing a tuning burden on the clinician. It must be shown, however, that the controller's benefits persist when deployed on a clinically-ready robotic prosthesis rather than on our prototype prosthesis. The translation of benefits is not guaranteed, as commercially-available robotic prostheses have many more practical design constraints than research prototypes, such as cost, weight, reliability, manufacturability, and more. These opposing constraints often result in a device that is more difficult to control due to more limited sensing and more complicated drivetrain dynamics. Further, robotic knee prostheses are most often paired with passive ankle/foot prostheses. The lack of an actuated ankle joint likely affects the overall behavior of the prosthesis during some activities, potentially affecting the efficacy of our controller.

This material is based on work supported by the National Institute of Child Health & Human Development of the National Institutes of Health under Award R01HD094772 and by the National Science Foundation under the Graduate Research Fellowship DGE 1841052. Prosthetic hardware and initial financial support were provided by Össur hf (Reykjavík, Iceland).

[1]Department of Robotics and [2]Department of Mechanical Engineering, University of Michigan, Ann Arbor, MI 48109. Contact: {tkbest, rdgregg}@umich.edu.

Therefore in this work, we detail and validate the deployment of our phase-based data-driven HKIC controller on the latest generation Össur Power Knee (PKA01) for sit/stand and level-ground walking tasks. After reviewing the Power Knee hardware and our HKIC controller from [5], [8], [11], we describe the updates made to the controller that account for the Power Knee's lack of ankle actuation and its non-negligible actuator dynamics. We then describe a series of experiments with N=4 high-mobility above-knee prosthesis users that highlight the clinical benefits of our controller on Power Knee compared with the users' prescribed passive devices in a series of stand-walk-sit experiments. Our preliminary results show that, despite different hardware properties compared to our research prosthesis, many of our controller's benefits persist across devices. Specifically, we demonstrate an increase in sit/stand speed and loading symmetry, similar to [8]. We also show improved walking gaits with increased early stance knee flexion and toe clearance. However, we also highlight instances in which the lack of an actuated ankle adversely affects the controller's biomimicry, such as in sit/stand. Overall, our results indicate our controller's ability to generalize to commercially-viable prostheses while retaining most of its clinical benefits.

II. Related Work

Previous research has tested the clinical benefits of commercially-available robotic prostheses, including earlier generations of the Össur Power Knee. Highsmith et al. presented a case study investigating sitting, standing, and walking on the first generation Power Knee [12]. The authors found that, for their participant, the Power Knee increased hip moment symmetry while sitting down compared to a C-Leg. However, no substantial symmetry improvement was observed at the knee joint or at all during standing. Wolf et al. similarly investigated the biomechanical differences in sit/stand when using the second generation Power Knee and the C-Leg, but observed "few differences between components and no effect on the intact limb" [13].

Most recently, Hafner et al. compared clinical outcomes between mechanical, microprocessor (Össur Rheo Knee™ II), and powered (second generation Össur Power Knee) prosthetic knees in an extensive 14 month randomized crossover trial with 12 participants [14]. The authors found that the Rheo Knee significantly improved the participants' mobility compared to mechanical knees and all of the participants elected to keep their Rheo Knee after the study. With the Power Knee, however, users demonstrated worse performance in the laboratory-based outcomes and the authors noted "high attrition of subjects", suggesting that users were unhappy with the powered device.

These three studies were unable to demonstrate compelling clinical benefits with the early models of the Power Knee, perhaps due to limitations in the prosthetic hardware, control software, or both. New, lighter and more compact commercialized robotic knees are now available, which may enable stronger clinical benefits. In this work therefore, we aim to again investigate the potential clinical benefits of commercialized robotic knees, but this time with modern hardware and a fundamentally different control approach that has previously shown benefits on a prototype prosthesis.

III. Prosthesis and Control System

A. Hardware Overview

In this study, we utilize the latest generation Power Knee from Össur (model PKA01), which is a commercialized robotic knee prosthesis. The drivetrain of the Power Knee consists of a brushless DC motor, a harmonic drive transmission, and a compliant linkage that connects the transmission output to the knee joint. The torque-angle relationship of the compliant linkage is nonlinear, stiffening under increasing deflection. The knee assembly weighs 2.7 kg (including battery) and the joint has a 120 deg range of motion. The removable lithium ion battery powers the motor and the embedded control electronics. The sensing suite includes joint and motor position encoders, a shank-mounted inertial measurement unit, and an array of ground reaction force (GRF) hall-effect sensors [27].

Based on the manufacturer's recommendations, we paired the Power Knee with the Pro-Flex® carbon fiber ankle-foot prosthesis. We used the Low Profile (LP) variety for all participants in order to maximize compatibility with different user heights and limb geometries. The appropriate size and category foot was used for each participant based on the sizing guidelines in the Pro-Flex LP Catalog. For a representative participant with average height and weight, the entire prosthesis, including the Power Knee, pylon, foot, shoe, and other hardware components, weighed 3.9 kg.

B. HKIC Controller Overview

In place of the Power Knee's stock control software, we also deployed a simplified version of our multi-activity phase-based HKIC controller [11], [28] for sit/stand and walking on the Power Knee (Fig. 1). This controller integrates the sit/stand and walk controllers from our research group's prior work [5], [8], using continuous, data-driven models of joint impedance and kinematics to produce biomimetic joint behavior for various activities. Our controller comprises two high-level modes: $\mu \in \{\text{Sit/Stand, Walk}\}$, which are automatically selected via a Finite State Machine (FSM). Simple, explainable transition rules based on the user's thigh motion control the transitions between modes (see Fig. 1 in [8] for further detail). A time-based interpolation between modal torque commands is used to smooth transitions between control modes over 100 ms.

In addition to the discrete mode μ, the controller calculates a continuous task variable χ and a continuous phase variable ϕ to evaluate the kinematic and impedance models (Fig. 1). In this initial translation to the Power Knee, we only include walking speed in the task variable χ, though other variables such as ground incline could be included in future iterations [5]. The phase variable $\phi \in [0, 1]$ quantifies the user's progression through either a walking gait cycle [5] or sitting and standing motions [8]. We calculate ϕ based on algebraic mappings of the user's thigh angle θ_{th}, giving

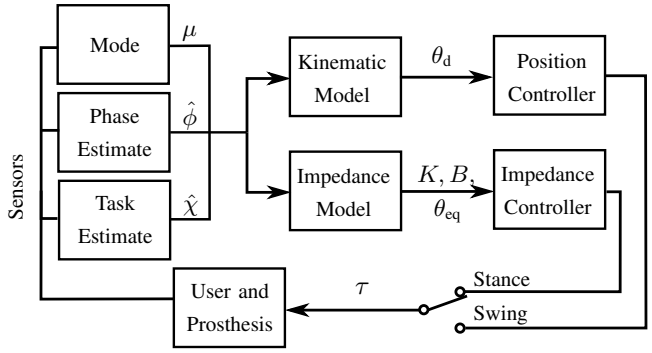

Fig. 1. A block diagram of the Hybrid Kinematic Impedance Controller used in this work. Real-time estimates of gait phase $\hat{\phi}$, task variation $\hat{\chi}$ (*i.e.* walking speed), and control mode μ (*i.e.* Walk vs. Sit/Stand) define desired joint impedance parameters K, B, θ_{eq} and joint angles θ_d using data-driven models. The torque commands τ are calculated using an impedance controller during stance or a position controller during swing.

them indirect volitional control over the prosthesis's behavior. The parameters used to calculate the phase variables adjust to the current task, allowing ϕ to appropriately parameterize the motion regardless of the varying thigh kinematics associated with different speeds and chair heights [19], [20].

While the user is in stance (which includes the entirety of Sit/Stand mode), the knee torque set point τ is calculated based on the joint angle θ_j and velocity $\dot{\theta}_j$ using impedance control:

$$\tau = K(\phi, \chi, \mu)\,[\theta_{eq}(\phi, \chi, \mu) - \theta_j] - B(\phi, \chi, \mu)\dot{\theta}_j, \quad (1)$$

where the stiffness K, damping B, and equilibrium angle θ_{eq} are functions of the phase variable ϕ, task variable χ, and mode μ. These parametric functions are fit offline to able-bodied training datasets [19], [21] such that (1) produces biomimetic joint torques when subjected to biomimetic joint kinematics. Details on the impedance model can be found in [5], [8].

Similarly, we use position control during the swing phase, where the desired joint angle θ_d and velocity $\dot{\theta}_d$ are modeled as functions of ϕ, χ, and μ. This kinematic model is likewise generated based on able-bodied kinematic data via convex optimization, with details in [29]. The knee torque is calculated through a proportional-derivative position controller as

$$\tau = k_p[\theta_d(\phi, \chi, \mu) - \theta_j] + k_d[\dot{\theta}_d(\phi, \chi, \mu) - \dot{\theta}_j], \quad (2)$$

where k_p and k_d are proportional and derivative gains, respectively. These gains are held constant across users.

C. HKIC Modifications for the Power Knee

In our previous work, our controllers have been mainly developed and evaluated using a prototype quasi-direct drive knee-ankle prosthesis [25]. While the Power Knee is distinct from this prototype prosthesis in many ways, there are two differences that are most relevant for control: 1) the Power Knee's drivetrain dynamics are more complex, and 2) the Power Knee does not have an actuated ankle joint. These differences impact how the knee joint should be controlled. We detail the modifications we made to our HKIC controller in response to each of these distinctions in turn below.

1) Low-Level Drivetrain Dynamics Compensation: Historically, the simple drivetrain dynamics of our original prototype prosthesis have allowed us to accurately control the joint impedance by assuming a proportional relationship between motor current and joint torque via the gear ratio and the motor's torque constant [25]. These assumptions are invalid on the Power Knee, as the design's high gear ratio and nonlinear series elasticity add substantial complexity to the drivetrain dynamics. For similar devices with these complex dynamics, such as the second generation Open-Source Leg [30], it has been shown that the motor inertia, series elasticity, and friction effects can introduce errors in the rendered joint impedance and ultimately errors in the produced joint torque [31], [32]. Further, it is well known in control theory that series elasticity can introduce stability problems when attempting to directly control joint position via non-collocated joint feedback [33]. Therefore, modifications to our original implementation are necessary in order to ensure accurate and stable impedance control on the Power Knee.

We utilize the approach presented in [32] to calculate optimal motor feedback gains that account for the drivetrain dynamics and minimize the rendered impedance error. Instead of calculating a motor torque setpoint using (1) and (2) directly, we use a collocated motor-space controller of the form

$$\tau = K_1(\theta_{eq,m} + \theta^* - \theta_m) - B_1\dot{\theta}_m, \quad (3)$$

where K_1 and B_1 are feedback gains that depend on the desired impedance K and B, the system parameters (inertia, viscous damping, etc.), and the transmission stiffness at the current transmission deflection. The motor states θ_m and $\dot{\theta}_m$ are decoupled from the joint states θ_j and $\dot{\theta}_j$ via the transmission elasticity. An offset angle θ^* is included to account for the transmission's nonlinear torque-angle relationship. Details on the calculation of K_1, B_1 and θ^* can be found in [32].

2) Unactuated Ankle Joint: Our previous work was performed using a prosthesis with an actuated ankle joint, allowing the ankle to behave biomimetically during all tasks. In contrast, the Pro-Flex foot used in conjunction with the Power Knee has fixed elastic properties that relate its ankle kinematics to ankle torques, constraining the space of producible behaviors. For level-ground walking, this added biomechanical constraint has comparatively little effect, as the Pro-Flex LP prosthesis is designed to primarily emulate level-ground walking biomechanics. For other activities however, normative ankle biomechanics deviate from this constraint curve in the torque-angle space, making it impossible for the passive prosthetic foot to replicate them.

One such activity in which the ankle biomechanics deviate substantially from the constraint curve is sit/stand. Average able-bodied seated data shows a moderately dorsiflexed ankle joint with zero ankle torque [21] (Fig. 2a). With a passive foot prosthesis and an unarticulated ankle joint however, the user cannot reach this low-torque, dorsiflexed configuration. They must instead choose between either a flat foot configuration with a vertical shank (Fig. 2b) or a non-flat foot configuration with an inclined shank (Fig. 2c).

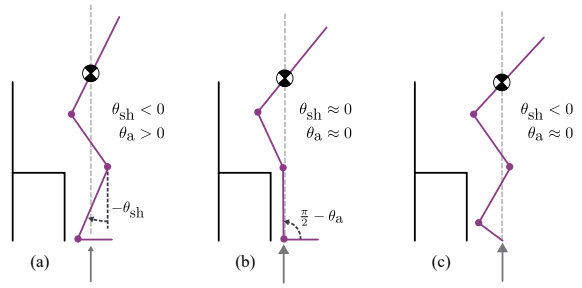

Fig. 2. A planar model of a person's foot, shank, thigh, and torso during the sit-to-stand motion in three possible configurations. The ground reaction force (gray arrow) is applied at the CoP, coinciding with the user's center of mass based on a quasi-static assumption. Tile (a) shows the nominal joint configurations used by able-bodied individuals, with $\theta_{sh} < 0, \theta_a > 0$, and the CoP located posterior to the knee joint center. Tiles (b) and (c) show the possible sit-to-stand configurations for a person using an above-knee prosthesis with a passive foot ($\theta_a \approx 0$), with either (b) a vertical shank ($\theta_{sh} \approx 0$) or (c) a non-flat foot ($\theta_{sh} < 0$).

Of the three configurations, the dorsiflexed configuration (Fig. 2a) is the most advantageous, as it allows the user to locate their center of pressure (CoP) posterior to the knee joint center. Assuming minimal anterior/posterior forces, it can be shown that the posterior separation of the CoP relative to the knee joint center prevents the foot/ankle complex from rotating off the ground (*i.e.* pivoting about the heel of the foot) when substantial knee torques are applied. The dorsiflexed configuration also helps prevent foot slipping, as the knee moment is opposed primarily by normal ground reaction forces rather than only by friction.

Of the two configurations available with a passive ankle, the inclined shank configuration (Fig. 2c) is most advantageous, as it does allow the CoP to be posterior to the knee joint, though only briefly. However, it requires the user to balance on the toe of the prosthesis during the motion, which may feel unstable. In our experience, most participants habitually use the configuration in Fig. 2b with their prescribed prostheses.

With a powered knee prosthesis, there is a risk of the applied knee extension torque producing negative consequences when the user elects to use the vertical shank configuration (Fig. 2b). If the CoP is too far anterior, the foot will rotate about the heel, sending the knee center backwards and potentially making the user lose their balance. Additionally, insufficient ground reaction force in this configuration may cause the knee torque to produce foot slipping rather than body weight support.

In response to this limitation caused by the unarticulated ankle joint, we modified our original sit/stand controller to prevent applying knee torques when the user elects to sit with a vertical shank (Fig. 2b). We scale the sit/stand knee stiffness and damping references with a unit logistic function of the user's shank angle θ_{sh}. The logistic mapping is defined as

$$\xi(\theta_{sh}) = \frac{1}{1 + e^{1.5(\theta_{sh}+2)}}, \tag{4}$$

where the angle constants have units of degrees. To prevent closed-loop oscillations that can occur from the interaction between the torque command and θ_{sh}, we low-pass filter θ_{sh} prior to (4). Since users typically adjust their posture slowly before standing, a 1 Hz cutoff frequency is sufficient to filter the signal without causing noticeable delays or response lag. As θ_{sh} increases above 0, the stiffness and damping asymptotically scale to 0, resulting in no knee joint torque. Conversely, as θ_{sh} decreases beyond 0, the logistic function approaches 1 and the stiffness and damping commands remain unchanged.

IV. Experimental Validation

To validate our controller's implementation on the Power Knee and to test for its clinical benefits, we recruited four participants with unilateral above-knee amputations (Table 1) to participate in our study. All participants were strong community ambulators (K4) and did not require mobility aids. The experimental protocol was approved by the University of Michigan Institutional Review Board (HUM00230065) and each participant provided informed consent.

A. Methods

We tested two conditions in this experiment over three sessions, with the participants using either 1) their prescribed prostheses (PRES), or 2) the Power Knee running our HKIC controller (PKNE). Each condition was tested on a separate day to mitigate fatigue effects, and the testing order was randomized to prevent procedural bias. Prior to the experiments, an acclimation day was provided during which the Power Knee prosthesis was fit and aligned to the participant by a certified prosthetist. The appropriate Pro-Flex LP foot was used for each participant based on their weight, activity level, and shoe size. The participant was taught how to use the Power Knee with the novel controller, and provided ample time to practice sitting, standing, and walking. The research team also provided coaching on how to best leverage the device's capabilities. This acclimation session lasted up to four hours.

The remaining two visits were identical aside from the prosthesis used (either PRES or PKNE). First, the participants were allowed to practice sitting, standing, and walking to warm up and re-familiarize themselves with the prosthesis.

TABLE 1
Enrolled Participant Details

Participant	Sex	Age (yrs)	Mass (kg)	Prescribed Prosthesis (Knee/Ankle)	Etiology	Amputation Type	Time Since Amputation (yrs)
TF01	M	23	79	Genium/Triton	Dysvascular Disease	Above Knee	10
TF02	M	25	84	Rheo/Proflex XC	Congenital	Knee Disartic.	24
TF03	M	20	75	Quattro/Shockwave	Cancer	Above Knee	2
TF04	F	42	66	X3/Triton LP	Trauma	Knee Disartic.	6

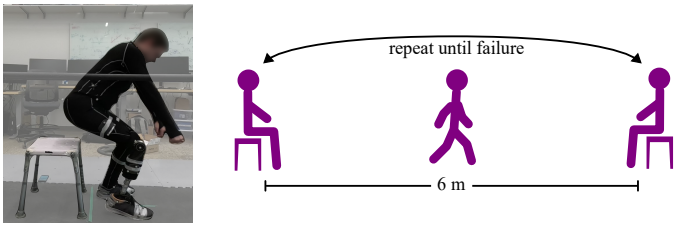

(a) (b)

Fig. 3. (a) A photo of participant TF01 standing from the first stool during the PKNE condition. (b) A graphical depiction of the incremental shuttle walk test protocol, depicting the participants walking between two stools approximately 6 m apart. Participants repeated walking between the stools until they could no longer keep up with the slowly increasing cued pace.

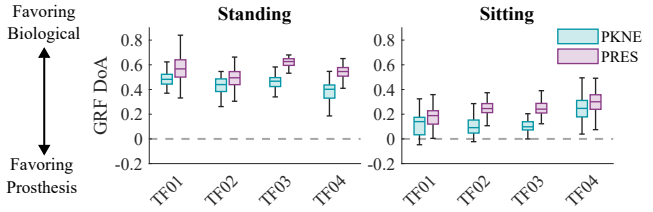

Fig. 4. Boxplots of the mean vertical GRF degree of asymmetry during sitting (left) and standing (right) for each participant. Values closer to zero indicate better GRF symmetry, whereas ± 1 indicate complete asymmetry.

Visual feedback during sit-stand was provided to allow the participants to practice symmetric limb loading, similar to [8]. This feedback was removed after the warm up period.

Next, the participants completed the main experiment, which involved completing repeated laps of an ambulation circuit consisting of two stools (45 cm tall) located approximately 6 m apart (Fig. 3). The protocol was inspired by the incremental shuttle walk test used to assess fitness in other domains [34], [35]. Handrails were provided along the walkway for safety, but their use was discouraged unless required to prevent a fall. Upon an auditory cue, participants stood up from a stool, walked to the opposite stool, turned around, and sat down to wait until the next cue. The cues were automated and followed this schedule: four cues at 65-second intervals, six at 43.3-second intervals, and eight at 32.5-second intervals, and so on, gradually increasing the minimum average walking pace from 0.1 m/s to 0.15 m/s and 0.2 m/s, respectively. The number of repetitions was chosen such that the total time at each pace was 260 s. Participants were allowed to choose their walking speed, but needed to reach the opposite stool before the next cue. The test ended if a participant failed to reach the stool on time for two consecutive laps.

During the experiments, motion capture and ground reaction force data were recorded (Vicon, Oxford, UK). These data were processed in OpenSim 4.5 (Stanford, CA, USA) using the model from Rajagopal et. al [36] with appropriate modifications made to the prosthetic side inertial properties, similar to [37]. Forceplates were located at each stool, allowing individual measurements of each leg's ground reaction force and inverse dynamics calculations. The walkway was not instrumented, and thus no walking joint kinetics were calculated.

In this work, we are only concerned with the non-rushed portions of the experiment (before the time between cues decreased substantially), as these are most similar to how our controller was previously tested on our prototype hardware. Therefore, we limit our analysis to the first 70 laps of the experiment. These early laps correspond to minimum average walking paces of ≤ 0.4 m/s and thus allow for "leisurely" activity completions without time pressure. Future work will analyze the latter portions of the experiment to investigate how performance changed under time pressure and with fatigue.

We segmented the experiment data from the first 70 laps into sitting, standing, transitioning, walking, and resting periods based on kinematic and force thresholds. We further divided the walking data into individual gait cycles based on the marker positions using methods from [38]. To examine whether the prosthesis condition had a statistically significant effect on the biomechanical measures of interest, we utilized linear mixed-effects models (LMMs). LMMs were chosen for their ability to include both fixed and random effects, allowing us to account for inter-participant variability. We treated the prosthesis condition (PRES or PKNE) as a fixed effect and the participant as a random intercept. Our null hypothesis posited that there would be no significant difference in these biomechanical measures between the prosthesis conditions, and our significance threshold was set to $\alpha = 0.05$.

B. Results

All participants were able to complete over 100 laps of the circuit with both their prescribed prostheses and the Power Knee, demonstrating the baseline functionality of our HKIC controller. The following subsections present results for the sitting/standing and walking portions of the circuit. For clarity in the presented boxplots, we excluded data points that are considered outliers, specifically those below Q1-1.5×IQR and above Q3+1.5×IQR.

1) Sitting and Standing: On the prototype hardware, our controller previously produced improved ground reaction force (GRF) symmetry [8]. We define the GFR degree of asymmetry DoA as

$$DoA = (F_\mathrm{b} - F_\mathrm{p})/(F_\mathrm{b} + F_\mathrm{p}), \tag{5}$$

where F_b and F_p are the vertical GRFs on the biological and prosthetic limbs, respectively. $DoA = 0$ indicates perfect GRF symmetry, whereas $DoA = 1$ and $DoA = -1$ indicate all force on the biological and prosthetic limbs, respectively. Similar to what was observed with the prototype hardware in [8], the mean GRF loading symmetry was improved in the PKNE condition compared to PRES condition for all participants (Fig. 4). The fit LMM showed an average DoA improvement of 11.6% for standing ($p < 0.001$) and 9.5% in sitting ($p < 0.001$) by the PKNE condition. Both conditions showed better sitting symmetry than standing symmetry.

We also calculated the time the participants took to perform the standing and sitting motions in each lap (Fig. 5). These timings only include the duration of the actual motions, excluding

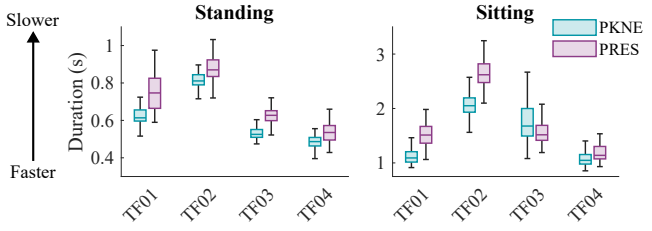

Fig. 5. Boxplots of the average duration of the sitting and standing motions during the experiment for each participant. The PKNE condition was significantly faster on average than the PRES condition.

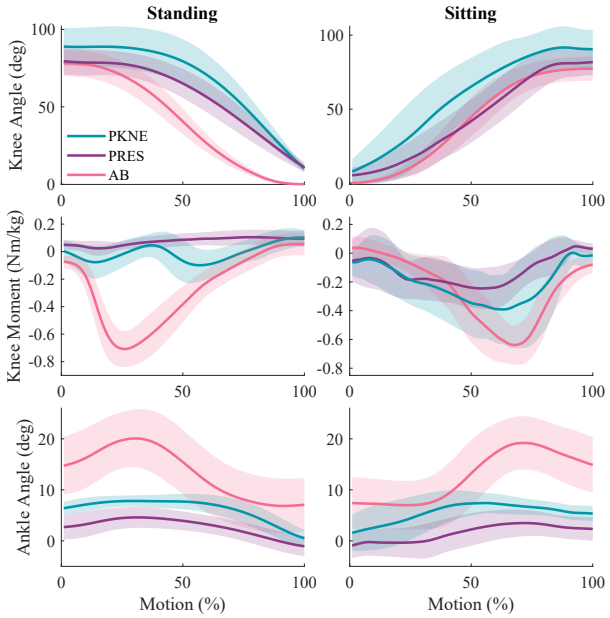

Fig. 6. Inter-participant average prosthetic-side joint kinematics and kinetics while sitting (left) and standing (right). Normative trajectories (AB) from [21] are shown as well for context. Ankle moments are excluded for brevity. Shaded regions represent ± 1 standard deviation.

transitions. On average, the PKNE condition produced faster motions than the PRES condition, with 11.9% ($p < 0.001$) and 13.0% ($p < 0.001$) reductions in standing and sitting times, respectively. Larger variance was observed in sitting, with some participants showing similar speed in both conditions.

We then compared the mean prosthetic knee and ankle kinematics and kinetics during sit/stand with normative able-bodied trajectories (Fig. 6). We did not plot the ankle moments, as they were small and their shape can be inferred from the kinematics due to the elastic nature of the prosthetic foot. Both conditions produced knee kinematics that are similar to able-bodied, with the PRES condition being the most similar in sitting. However, the ankle kinematics produced by either condition's passive feet differ substantially from the normative trajectories, likely impacting the knee's behavior. The knee moments in sitting are more similar to able-bodied for the PKNE condition than for the PRES condition. While the standing knee moments for PKNE are also closer to able-bodied than the PRES condition, they are still not as biomimetic as what was observed in [8], likely due to the

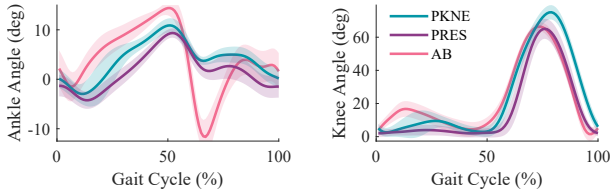

Fig. 7. Inter-participant average kinematic trajectories of the prosthetic joints during the overground walking portions of the experiment. Mean able-bodied trajectories (AB) of 1.0 m/s walking from [19] are also plotted for reference. Shaded regions represent ± 1 standard deviation.

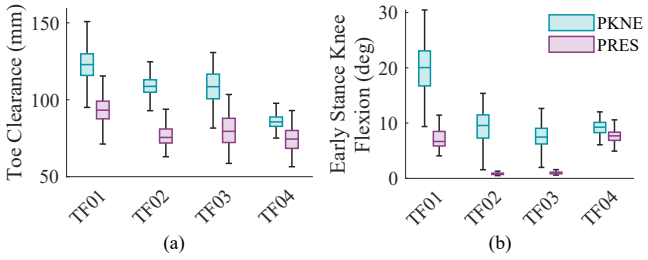

Fig. 8. Boxplots of the average kinematic features during the overground walking portions of the experiments. Tile (a) shows the minimum toe clearance during swing and tile (b) shows the peak early stance knee flexion.

configuration mismatch caused by the passive ankle and our control modification to taper knee torque as $\theta_{sh} \to 0$.

2) Overground Walking: Like in sit/stand, we compared the mean prosthetic knee and ankle kinematics with normative able-bodied trajectories (Fig. 7), as previous experiments with the prototype hardware demonstrated improved biomimicry [5]. Qualitatively, the kinematics at both joints were reasonably similar to able-bodied for both conditions, with a few notable differences in key kinematic features. The PKNE condition showed slightly larger peak ankle dorsiflexion angles, suggesting more energy storage in the prosthetic foot available for push off. The PKNE condition also showed increased peak swing knee flexion angles (mean $\approx$ 76 deg). The peak knee flexion angle in the HKIC controller's kinematic model is $\approx$ 68 deg, indicating that the observed extra flexion was caused by natural swing dynamics rather than explicit control effort. Though less biomimetic, the increased knee flexion was likely beneficial in increasing the toe clearance during swing (Fig. 8a). We calculated this toe clearance based on the minimum position of the 1st and 5th metatarsal markers during mid-swing. On average, the PKNE condition produced 25.5 mm (31.4%) more toe clearance than the PRES condition ($p < 0.001$). An increase in early stance knee flexion was also observed in the PKNE condition (Fig. 8b), with one participant approaching the average able-bodied amount of 16.5 deg. On average, the PKNE condition produced 7.4 deg (172.8%) more early stance knee flexion than the PRES condition ($p < 0.001$).

Finally, we calculated the step length symmetry index for each stride and condition, defined as ratio between the prosthetic and the subsequent biological leg step lengths. A step length symmetry index of 1 corresponds to perfectly symmetric step lengths, while values greater than 1 indicate

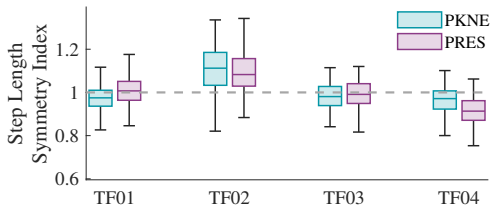

Fig. 9. Mean step length symmetry index for each participant and condition during the overground walking portions of the experiment. Perfectly equal step lengths would result in a symmetry index of 1, whereas values greater than 1 indicate longer steps with the prosthesis.

longer steps with the prosthesis. Shown in Fig. 9, no significant relationship between the prosthesis condition and step length symmetry was observed ($p = 0.54$).

V. Discussion

Many, but not all, of the clinical benefits observed on the prototype hardware in [5], [8] transferred with the HKIC to the Power Knee. The improved GRF symmetry during sit/stand observed in the PKNE condition is an important clinical result, as the better sharing of the GRF between limbs will likely reduce overuse injuries over time. Further, while the speed increase is not directly clinically relevant, it is likely indicative of the sit/stand motions being easier to perform with the PKNE condition than the PRES condition.

However, these effects are not as large as they were previously in [8], likely due to configuration mismatches caused by the passive ankle (Fig. 2). In particular, the standing knee moments produced by the PKNE condition were not as biomimetic as they had been previously (Fig. 6). We hypothesize that this is due, in part, to the difficulty of maintaining the Fig. 2c configuration. Participants often reverted to the vertical shank configuration, in which our controller does not apply knee torque in order to avoid slipping. Systematically characterizing the effects of a non-articulated ankle in sit/stand is an interesting avenue for future work.

In the overground walking portions of the experiment, we observed improvements in key kinematic gait features. The increased toe clearance in the PKNE condition (Fig. 8a), which likely resulted from the increased peak swing knee flexion (Fig. 7), is beneficial for real-world use, as mid-swing trips are a common source of falls [39]. Importantly, the participants did not note any disadvantages of the increased toe clearance or swing knee flexion. The PKNE condition also created more early stance knee flexion than the PRES condition, though not quite to the extent of normative able-bodied gait. Early stance knee flexion is desirable, as it can absorb heelstrike impacts and allow individuals to better maintain forward momentum [40]. Although the prescribed MPKs used by the participants all support early stance knee flexion, the participants did not appear to leverage this feature in the PRES condition.

Though promising, this initial study is not without limitations. First, our study cohort represents only a limited segment of the population, which restricts the generalizability of our findings. The participants were all high-activity (K4) ambulators, and it is possible that our results are unique to this demographic. For instance, related work in robotic ankle prostheses found that higher mobility groups benefited more from the robotic assistance compared to those with lower mobility [41]. Future work is required to understand the PKNE condition's effects across broader populations.

Furthermore, our experiments did not capture all aspects of everyday prosthesis use. For example, we tested only a portion of the activities that occur in real-world ambulation, neglecting activities such as stair traversal. Experiments testing the generalization of our stairs controller [23] should be performed as well. Additionally, we provided limited training and acclimation to the novel device, whereas the participants were extremely acclimated to their PRES prostheses. In real-world use, the acclimation levels across conditions would be more balanced. As our controller matures and becomes appropriate for take-home use, a more comprehensive experiment with longer acclimation and testing horizons should be performed, similar to [14].

Finally, the extent to which the HKIC control methodology independently influenced the observed outcomes was not tested in our experiments. Future work should compare results between the Power Knee under HKIC control to those created with its default control behavior to isolate these effects.

VI. Conclusion

In this article, we presented the first implementation of a phase-variable impedance controller on the Össur Power Knee, utilizing data-driven impedance and kinematic models in place of FSM control. In preliminary experiments involving walking and sit/stand, we showed that many of the clinical benefits that we observed with the same control approach on prototype hardware generalized to the Power Knee. By demonstrating compelling evidence of clinical benefits on commercially-viable prosthesis hardware such as the Power Knee, we aim to help accelerate the adoption of robotic knee-ankle prostheses into mainstream clinical practice.

Acknowledgments

The authors would like to thank Jeffrey Wensman, CPO for providing clinical support, Atli Örn Sverrisson and David Langlois for assistance with the Power Knee hardware, Dr. Ryan Posh for providing valuable feedback on the manuscript, and our dedicated participants for making this work possible.

Conflict of Interest Disclosure

TKB and RDG have applied for patents related to the HKIC control method.

This research received initial funding from Össur ehf (Reykjavík, Iceland), which may have a financial interest in the outcomes of this study. The authors independently conducted the research and analysis, and the results and conclusions presented in this paper are those of the authors alone. These findings do not necessarily reflect the views or positions of Össur ehf, the National Science Foundation, or the National Institutes of Health.

REFERENCES

[1] R. Gehlhar, M. Tucker, A. J. Young, and A. D. Ames, "A review of current state-of-the-art control methods for lower-limb powered prostheses," *Annu. Rev. Control.*, vol. 55, pp. 142–164, 2023.

[2] I. Fagioli, A. Mazzarini, C. Livolsi, E. Gruppioni, N. Vitiello, S. Crea, and E. Trigili, "Advancements and Challenges in the Development of Robotic Lower Limb Prostheses: a Systematic Review," *IEEE Trans. Med. Robot. and Bionics*, vol. PP, no. 99, pp. 1–1, 2024.

[3] C. Jayaraman, S. Hoppe-Ludwig, S. Deems-Dluhy, M. McGuire, C. Mummidisetty, R. Siegal, A. Naef, B. E. Lawson, M. Goldfarb, K. E. Gordon, and A. Jayaraman, "Impact of Powered Knee-Ankle Prosthesis on Low Back Muscle Mechanics in Transfemoral Amputees: A Case Series," *Frontiers in Neuroscience*, vol. 12, p. 134, 2018.

[4] M. Tran, L. Gabert, S. Hood, and T. Lenzi, "A lightweight robotic leg prosthesis replicating the biomechanics of the knee, ankle, and toe joint," *Science Robotics*, vol. 7, no. 72, p. eabo3996, 2022.

[5] T. K. Best, C. G. Welker, E. J. Rouse, and R. D. Gregg, "Data-driven variable impedance control of a powered knee–ankle prosthesis for adaptive speed and incline walking," *IEEE Trans. Robot.*, vol. 39, no. 3, pp. 2151–2169, 2023.

[6] A. M. Simon, N. P. Fey, K. A. Ingraham, S. B. Finucane, E. G. Halsne, and L. J. Hargrove, "Improved Weight-Bearing Symmetry for Transfemoral Amputees during Standing Up and Sitting Down with a Powered Knee-Ankle Prosthesis," *Arch. of Phys. Med. and Rehab.*, vol. 97, pp. 1100–1106, 2016.

[7] G. Hunt, S. Hood, and T. Lenzi, "Stand-Up, Squat, Lunge, and Walk with a Robotic Knee and Ankle Prosthesis under Shared Neural Control," *IEEE Open J. Eng. Med. Biol.*, vol. 2, pp. 267–277, 2021.

[8] C. G. Welker, T. K. Best, R. D. Gregg, and C. G. Welker, "Improving Sit/Stand Loading Symmetry and Timing Through Unified Variable Impedance Control of a Powered Knee-Ankle Prosthesis," *IEEE Trans. Neural Syst. Rehabil. Eng.*, vol. 31, pp. 4146–4155, 2023.

[9] E. C. Martinez-Villalpando, L. Mooney, G. Elliott, and H. Herr, "Antagonistic Active Knee Prosthesis. A Metabolic Cost of Walking Comparison With a Variable-Damping Prosthetic Knee," *Conf. Proc. IEEE Eng. Med. Biol. Soc.*, vol. 2011, pp. 8519–8522, 2011.

[10] E. D. Ledoux and M. Goldfarb, "Control and evaluation of a powered transfemoral prosthesis for stair ascent," *IEEE Trans. Neural Syst. Rehabilitation Eng.*, vol. 25, 2017.

[11] T. K. Best, C. A. Laubscher, R. J. Cortino, S. Cheng, and R. D. Gregg, "Improving amputee endurance over activities of daily living with a robotic knee-ankle prosthesis: A case study," in *IEEE/RSJ Int. Conf. Intell. Robots Syst.*, 2023, pp. 2101–2107.

[12] M. J. Highsmith, J. T. Kahle, S. L. Carey, D. J. Lura, R. V. Dubey, and W. S. Quillen, "Kinetic Differences Using a Power Knee and C-Leg While Sitting Down and Standing Up: A Case Report," *J. Prosthetics and Orthotics*, vol. 22, no. 4, pp. 237–243, 2010.

[13] E. J. Wolf, V. Q. Everding, A. A. Linberg, J. M. Czerniecki, and C. J. M. Gambel, "Comparison of the Power Knee and C-Leg during step-up and sit-to-stand tasks," *Gait & Posture*, vol. 38, no. 3, pp. 397–402, 2013.

[14] B. J. Hafner and R. L. Askew, "Physical performance and self-report outcomes associated with use of passive, adaptive, and active prosthetic knees in persons with unilateral, transfemoral amputation: Randomized crossover trial," *J. Rehabil. Res. Dev.*, vol. 52, no. 6, pp. 677–700, 2015.

[15] F. Sup, A. Bohara, and M. Goldfarb, "Design and control of a powered transfemoral prosthesis," *The Int. J. of Robotics Research*, vol. 27, no. 2, pp. 263–273, 2008.

[16] A. M. Simon, K. A. Ingraham, N. P. Fey, S. B. Finucane, R. D. Lipschutz, A. J. Young, and L. J. Hargrove, "Configuring a powered knee and ankle prosthesis for transfemoral amputees within five specific ambulation modes," *PLoS One*, vol. 9, no. 6, 2014.

[17] H. Huang, D. L. Crouch, M. Liu, G. S. Sawicki, and D. Wang, "A Cyber Expert System for Auto-Tuning Powered Prosthesis Impedance Control Parameters," *Ann. Biomed. Eng.*, vol. 44, no. 5, pp. 1613–1624, 2016.

[18] R. Wu, M. Li, Z. Yao, W. Liu, J. Si, and H. Huang, "Reinforcement learning impedance control of a robotic prosthesis to coordinate with human intact knee motion," *IEEE Robotics and Automation Letters*, vol. 7, no. 3, pp. 7014–7020, 2022.

[19] E. Reznick, K. R. Embry, R. Neuman, E. Bolívar-Nieto, N. P. Fey, and R. D. Gregg, "Lower-limb kinematics and kinetics during continuously varying human locomotion," *Sci. Data*, vol. 8, 2021.

[20] J. Camargo, A. Ramanathan, W. Flanagan, and A. Young, "A comprehensive, open-source dataset of lower limb biomechanics in multiple conditions of stairs, ramps, and level-ground ambulation and transitions," *J. Biomech.*, vol. 119, p. 110320, 2021.

[21] J. Vantilt *et al.*, "Model-based control for exoskeletons with series elastic actuators evaluated on sit-to-stand movements," *J. NeuroEng. Rehabil.*, vol. 16, no. 65, Jun. 2019.

[22] T. K. Best, K. Embry, E. J. Rouse, and R. D. Gregg, "Phase-variable control of a powered knee-ankle prosthesis over continuously varying speeds and inclines," *IEEE Int. Conf. Intelli. Robot. Sys.*, 2021.

[23] R. J. Cortino, T. K. Best, and R. D. Gregg, "Data-driven phase-based control of a powered knee-ankle prosthesis for variable-incline stair ascent and descent," *IEEE Trans. Med. Robot. Bionics*, vol. 6, no. 1, pp. 175–188, 2024.

[24] S. Cheng, C. A. Laubscher, and R. D. Gregg, "Controlling Powered Prosthesis Kinematics over Continuous Inter-Leg Transitions Between Walking and Stair Ascent/Descent," *IEEE Trans. Neural Syst. Rehabil. Eng.*, vol. PP, no. 99, pp. 1–1, 2024.

[25] T. Elery, S. Rezazadeh, C. Nesler, and R. D. Gregg, "Design and validation of a powered knee-ankle prosthesis with high-torque, low-impedance actuators," *IEEE Trans. Robot.*, vol. 36, no. 6, pp. 1649–1668, 2020.

[26] S. Cheng, C. A. Laubscher, R. D. Gregg, and S. Cheng, "Automatic Stub Avoidance for a Powered Prosthetic Leg Over Stairs and Obstacles," *IEEE Trans. Biomed. Eng.*, vol. 71, no. 5, pp. 1499–1510, 2024.

[27] S. Gudjonsson, Á. Einarsson, H. I. Thorsteinsdottir, and D. Langlois, "Ground contact sensor array for lower-limb prosthetic and orthotic devices," U.S. Patent Application US20 220 401 236A1, 2022.

[28] S. Cheng, C. A. Laubscher, T. K. Best, and R. D. Gregg, "Ambilateral activity recognition and continuous adaptation with a powered knee-ankle prosthesis," *IEEE Transactions on Robotics*, pp. 1–17, 2025.

[29] K. Embry, D. J. Villarreal, R. L. Macaluso, and R. D. Gregg, "Modeling the Kinematics of Human Locomotion over Continuously Varying Speeds and Inclines," *IEEE Trans. Neural Syst. Rehabil. Eng.*, vol. 26, no. 12, pp. 2342–2350, 2018.

[30] S. Ayyappan and E. Rouse. (2023) The Open Source Leg. [Online]. Available: https://www.opensourceleg.org/build

[31] A. F. Azocar and E. J. Rouse, "Characterization of Open-loop Impedance Control and Efficiency in Wearable Robots," *IEEE Robot. Autom. Lett.*, vol. 7, no. 2, pp. 4313–4320, 2022.

[32] T. K. Best, G. C. Thomas, S. R. Ayyappan, R. D. Gregg, and E. J. Rouse, "A Compensated Open-Loop Impedance Controller Evaluated on the Second-Generation Open-Source Leg Prosthesis," *Under Review.*, 2024.

[33] M. W. Spong, S. Hutchinson, and M. Vidyasagar, *Robot Modeling and Control (2nd Edition)*. Wiley, 2020.

[34] F. J. Morales, A. Martínez, M. Méndez, A. Agarrado, F. Ortega, J. Fernández-Guerra, T. Montemayor, and J. Burgos, "A shuttle walk test for assessment of functional capacity in chronic heart failure," *Am. Heart J.*, vol. 138, no. 2, pp. 291–298, 1999.

[35] M. T. Mahar, A. M. Guerieri, M. S. Hanna, and C. D. Kemble, "Estimation of Aerobic Fitness from 20-m Multistage Shuttle Run Test Performance," *Am. J. Preventive Medicine*, vol. 41, no. 4, pp. S117–S123, 2011.

[36] A. Rajagopal, C. L. Dembia, M. S. DeMers, D. D. Delp, J. L. Hicks, and S. L. Delp, "Full-body musculoskeletal model for muscle-driven simulation of human gait," *IEEE Trans. Biomed. Eng.*, vol. 63, no. 10, pp. 2068–2079, 2016.

[37] V. Raveendranathan, V. G. M. Kooiman, and R. Carloni, "Musculoskeletal model of osseointegrated transfemoral amputees in OpenSim," *PLOS ONE*, vol. 18, no. 9, p. e0288864, 2023.

[38] J. Zeni, J. Richards, and J. Higginson, "Two simple methods for determining gait events during treadmill and overground walking using kinematic data," *Gait & Posture*, vol. 27, no. 4, pp. 710–714, 2008.

[39] J. Kim, C. L. McDonald, B. J. Hafner, and A. Sawers, "Fall-related events in people who are lower limb prosthesis users: the lived experience," *Disabil. Rehabil.*, vol. 44, no. 15, pp. 3897–3908, 2022.

[40] J. Perry, J. Burnfield, and L. Cabico, *Gait Analysis: Normal and Pathological Function*, 2nd ed. Thorofare, NJ: Slack, 2010.

[41] E. S. Gardinier, B. M. Kelly, J. Wensman, and D. H. Gates, "A controlled clinical trial of a clinically-tuned powered ankle prosthesis in people with transtibial amputation," *Clinical Rehabilitation*, vol. 32, no. 3, pp. 319–329, 2017.